

# ENPM667 Final Project)

Che-Jung Chuang, Giang-Nam Facchetti, David Ajayi

December 2025

## 1 First Component, Part A: Nonlinear Modeling of the Double-Pendulum Crane

In this section, the nonlinear equations of motion of the crane system with two suspended loads are derived using Lagrange's method, and the result is written in nonlinear state-space form.

### 1.1 Generalized Coordinates and Kinematics

The system consists of a cart of mass  $M$  moving horizontally on a frictionless rail, with two point masses  $m_1$  and  $m_2$  suspended from the cart by massless, rigid links of lengths  $l_1$  and  $l_2$ , respectively. The input to the system is a horizontal force  $F(t)$  applied to the cart.

A Cartesian inertial frame is fixed such that the  $x$ -axis is horizontal (positive to the right) and the  $y$ -axis is vertical (positive downward). The generalized coordinates are chosen as

$$q_1 = x(t), \quad q_2 = \theta_1(t), \quad q_3 = \theta_2(t),$$

where  $x(t)$  denotes the horizontal position of the cart, and  $\theta_i(t)$ ,  $i = 1, 2$ , denote the angular displacements of the pendulum links measured from the vertical downward direction (counterclockwise positive).

With this convention, the Cartesian coordinates of the cart and the two point masses are

$$x_C = x, \quad y_C = 0, \quad (1)$$

$$x_1 = x + l_1 \sin \theta_1, \quad y_1 = l_1 \cos \theta_1, \quad (2)$$

$$x_2 = x + l_2 \sin \theta_2, \quad y_2 = l_2 \cos \theta_2. \quad (3)$$

Differentiating with respect to time yields the corresponding velocities:

$$\dot{x}_C = \dot{x}, \quad \dot{y}_C = 0, \quad (4)$$

$$\dot{x}_1 = \dot{x} + l_1 \cos \theta_1 \dot{\theta}_1, \quad \dot{y}_1 = -l_1 \sin \theta_1 \dot{\theta}_1, \quad (5)$$

$$\dot{x}_2 = \dot{x} + l_2 \cos \theta_2 \dot{\theta}_2, \quad \dot{y}_2 = -l_2 \sin \theta_2 \dot{\theta}_2. \quad (6)$$

### 1.2 Kinetic and Potential Energy

The total kinetic energy  $T$  of the system is the sum of the kinetic energies of the cart and the two point masses:

$$T = \frac{1}{2} M \dot{x}^2 + \frac{1}{2} m_1 (\dot{x}_1^2 + \dot{y}_1^2) + \frac{1}{2} m_2 (\dot{x}_2^2 + \dot{y}_2^2). \quad (7)$$

Using the velocity expressions above,

$$\begin{aligned} \dot{x}_1^2 + \dot{y}_1^2 &= (\dot{x} + l_1 \cos \theta_1 \dot{\theta}_1)^2 + (-l_1 \sin \theta_1 \dot{\theta}_1)^2 \\ &= \dot{x}^2 + 2l_1 \cos \theta_1 \dot{x} \dot{\theta}_1 + l_1^2 \dot{\theta}_1^2 (\cos^2 \theta_1 + \sin^2 \theta_1) \\ &= \dot{x}^2 + 2l_1 \cos \theta_1 \dot{x} \dot{\theta}_1 + l_1^2 \dot{\theta}_1^2, \end{aligned} \quad (8)$$

and similarly

$$\dot{x}_2^2 + \dot{y}_2^2 = \dot{x}^2 + 2l_2 \cos \theta_2 \dot{x} \dot{\theta}_2 + l_2^2 \dot{\theta}_2^2. \quad (9)$$

Substituting into  $T$  and collecting terms gives

$$\begin{aligned} T &= \frac{1}{2} M \dot{x}^2 + \frac{1}{2} m_1 \left( \dot{x}^2 + 2l_1 \cos \theta_1 \dot{x} \dot{\theta}_1 + l_1^2 \dot{\theta}_1^2 \right) \\ &\quad + \frac{1}{2} m_2 \left( \dot{x}^2 + 2l_2 \cos \theta_2 \dot{x} \dot{\theta}_2 + l_2^2 \dot{\theta}_2^2 \right) \\ &= \frac{1}{2} (M + m_1 + m_2) \dot{x}^2 + m_1 l_1 \cos \theta_1 \dot{x} \dot{\theta}_1 + m_2 l_2 \cos \theta_2 \dot{x} \dot{\theta}_2 \\ &\quad + \frac{1}{2} m_1 l_1^2 \dot{\theta}_1^2 + \frac{1}{2} m_2 l_2^2 \dot{\theta}_2^2. \end{aligned} \quad (10)$$

The gravitational potential energy  $V$  is computed with the  $y$ -axis pointing downward, so that

$$V = m_1 g y_1 + m_2 g y_2 = m_1 g l_1 \cos \theta_1 + m_2 g l_2 \cos \theta_2, \quad (11)$$

where  $g$  is the gravitational acceleration.

### 1.3 Lagrangian and Euler–Lagrange Equations

The Lagrangian of the system is defined as

$$L(q, \dot{q}) = T - V. \quad (12)$$

Using the generalized coordinates

$$q_1 = x, \quad q_2 = \theta_1, \quad q_3 = \theta_2,$$

the equations of motion follow from the Euler–Lagrange equations

$$\frac{d}{dt} \left( \frac{\partial L}{\partial \dot{q}_i} \right) - \frac{\partial L}{\partial q_i} = Q_i, \quad i = 1, 2, 3, \quad (13)$$

where  $Q_i$  denotes the generalized force associated with  $q_i$ .

The external horizontal force  $F(t)$  acts directly on the cart coordinate  $x$ , so

$$Q_x = F, \quad Q_{\theta_1} = 0, \quad Q_{\theta_2} = 0. \quad (14)$$

Carrying out the partial derivatives and time derivatives for each generalized coordinate leads to the following coupled, second-order nonlinear equations of motion:

**Cart translation:**

$$(M + m_1 + m_2) \ddot{x} + m_1 l_1 (\ddot{\theta}_1 \cos \theta_1 - \dot{\theta}_1^2 \sin \theta_1) + m_2 l_2 (\ddot{\theta}_2 \cos \theta_2 - \dot{\theta}_2^2 \sin \theta_2) = F. \quad (15)$$

**First pendulum:**

$$l_1 \ddot{\theta}_1 + \ddot{x} \cos \theta_1 + g \sin \theta_1 = 0. \quad (16)$$

**Second pendulum:**

$$l_2 \ddot{\theta}_2 + \ddot{x} \cos \theta_2 + g \sin \theta_2 = 0. \quad (17)$$

Equations (15)–(17) represent the nonlinear dynamics of the double-pendulum crane system.

## 1.4 Explicit Form of the Accelerations

Equations (16) and (17) can be solved for  $\ddot{\theta}_1$  and  $\ddot{\theta}_2$  in terms of  $\ddot{x}$ :

$$\ddot{\theta}_1 = -\frac{\ddot{x} \cos \theta_1 + g \sin \theta_1}{l_1}, \quad (18)$$

$$\ddot{\theta}_2 = -\frac{\ddot{x} \cos \theta_2 + g \sin \theta_2}{l_2}. \quad (19)$$

Substituting (18)–(19) into the cart equation (15) and simplifying yields

$$\ddot{x} = \frac{F + m_1(g \cos \theta_1 + l_1 \dot{\theta}_1^2) \sin \theta_1 + m_2(g \cos \theta_2 + l_2 \dot{\theta}_2^2) \sin \theta_2}{M + m_1 \sin^2 \theta_1 + m_2 \sin^2 \theta_2}. \quad (20)$$

Using (20) in (18) and (19), the angular accelerations become

$$\ddot{\theta}_1 = -\frac{\ddot{x} \cos \theta_1 + g \sin \theta_1}{l_1}, \quad (21)$$

$$\ddot{\theta}_2 = -\frac{\ddot{x} \cos \theta_2 + g \sin \theta_2}{l_2}, \quad (22)$$

where  $\ddot{x}$  is given by (20).

## 1.5 Nonlinear State-Space Representation

For control design and simulation, it is convenient to write the dynamics in first-order state-space form. The state vector is defined as

$$\mathbf{x} = \begin{bmatrix} x_1 \\ x_2 \\ x_3 \\ x_4 \\ x_5 \\ x_6 \end{bmatrix} = \begin{bmatrix} x \\ \dot{x} \\ \theta_1 \\ \dot{\theta}_1 \\ \theta_2 \\ \dot{\theta}_2 \end{bmatrix}, \quad u = F. \quad (23)$$

Using the definitions above, the first-order dynamics are

$$\dot{x}_1 = x_2, \quad (24)$$

$$\dot{x}_2 = \ddot{x} = \frac{u + m_1(g \cos x_3 + l_1 x_4^2) \sin x_3 + m_2(g \cos x_5 + l_2 x_6^2) \sin x_5}{M + m_1 \sin^2 x_3 + m_2 \sin^2 x_5}, \quad (25)$$

$$\dot{x}_3 = x_4, \quad (26)$$

$$\dot{x}_4 = \ddot{\theta}_1 = -\frac{\dot{x}_2 \cos x_3 + g \sin x_3}{l_1}, \quad (27)$$

$$\dot{x}_5 = x_6, \quad (28)$$

$$\dot{x}_6 = \ddot{\theta}_2 = -\frac{\dot{x}_2 \cos x_5 + g \sin x_5}{l_2}. \quad (29)$$

Equations (24)–(29) define the nonlinear state-space model

$$\dot{\mathbf{x}} = f(\mathbf{x}, u) \quad (30)$$

of the double-pendulum crane, with state  $\mathbf{x} \in \mathbb{R}^6$  and control input  $u = F$ .

## 2 First Component, Part B: Linearization via Jacobians

### 2.1 Nonlinear State-Space Model and Equilibrium

From Part A, the nonlinear dynamics of the double-pendulum crane can be written in state-space form as

$$\dot{\mathbf{x}} = f(\mathbf{x}, u), \quad (31)$$

with state and input

$$\mathbf{x} = \begin{bmatrix} x_1 \\ x_2 \\ x_3 \\ x_4 \\ x_5 \\ x_6 \end{bmatrix} = \begin{bmatrix} x \\ \dot{x} \\ \theta_1 \\ \dot{\theta}_1 \\ \theta_2 \\ \dot{\theta}_2 \end{bmatrix}, \quad u = F. \quad (32)$$

Using the shorthand

$$D(\mathbf{x}) = M + m_1 \sin^2 x_3 + m_2 \sin^2 x_5, \quad (33)$$

the components of  $f(\mathbf{x}, u)$  are

$$f_1(\mathbf{x}, u) = x_2, \quad (34)$$

$$f_2(\mathbf{x}, u) = \ddot{x} = \frac{u + m_1(g \cos x_3 + l_1 x_4^2) \sin x_3 + m_2(g \cos x_5 + l_2 x_6^2) \sin x_5}{D(\mathbf{x})}, \quad (35)$$

$$f_3(\mathbf{x}, u) = x_4, \quad (36)$$

$$f_4(\mathbf{x}, u) = \ddot{\theta}_1 = -\frac{f_2(\mathbf{x}, u) \cos x_3 + g \sin x_3}{l_1}, \quad (37)$$

$$f_5(\mathbf{x}, u) = x_6, \quad (38)$$

$$f_6(\mathbf{x}, u) = \ddot{\theta}_2 = -\frac{f_2(\mathbf{x}, u) \cos x_5 + g \sin x_5}{l_2}. \quad (39)$$

The operating condition of interest is the configuration where the cart is at the origin and both pendulums hang vertically downward with zero velocities and zero input. The corresponding equilibrium is

$$\mathbf{x}_e = \begin{bmatrix} 0 \\ 0 \\ 0 \\ 0 \\ 0 \\ 0 \end{bmatrix}, \quad u_e = 0, \quad (40)$$

and it satisfies  $f(\mathbf{x}_e, u_e) = \mathbf{0}$ .

Deviation variables are defined as

$$\delta \mathbf{x} = \mathbf{x} - \mathbf{x}_e, \quad \delta u = u - u_e. \quad (41)$$

Since the equilibrium is located at the origin, these deviations coincide with the physical variables, and the notation below omits the explicit  $\delta$  for simplicity.

## 2.2 Jacobian Linearization

The linearization of the nonlinear system around  $(\mathbf{x}_e, u_e)$  is obtained by a first-order Taylor expansion of  $f(\mathbf{x}, u)$ :

$$\dot{\mathbf{x}} = f(\mathbf{x}, u) \approx f(\mathbf{x}_e, u_e) + \left. \frac{\partial f}{\partial \mathbf{x}} \right|_{(\mathbf{x}_e, u_e)} (\mathbf{x} - \mathbf{x}_e) + \left. \frac{\partial f}{\partial u} \right|_{(\mathbf{x}_e, u_e)} (u - u_e). \quad (42)$$

Using  $f(\mathbf{x}_e, u_e) = \mathbf{0}$  and  $\mathbf{x}_e = \mathbf{0}, u_e = 0$ , this reduces to

$$\dot{\mathbf{x}} \approx A \mathbf{x} + B u, \quad A = \left. \frac{\partial f}{\partial \mathbf{x}} \right|_{(\mathbf{x}_e, u_e)}, \quad B = \left. \frac{\partial f}{\partial u} \right|_{(\mathbf{x}_e, u_e)}. \quad (43)$$

The matrices  $A$  and  $B$  are the Jacobians of  $f(\mathbf{x}, u)$  with respect to the state and input, evaluated at the equilibrium.

## 2.3 Computation of the Jacobians

The Jacobian  $A$  is assembled from the partial derivatives

$$A_{ij} = \frac{\partial f_i}{\partial x_j} \Big|_{(\mathbf{x}_e, u_e)}, \quad i, j = 1, \dots, 6.$$

**First and third rows.** From (34) and (36),

$$f_1 = x_2, \quad f_3 = x_4,$$

so the only nonzero derivatives are

$$\frac{\partial f_1}{\partial x_2} = 1, \quad \frac{\partial f_3}{\partial x_4} = 1, \quad (44)$$

and all other partial derivatives of  $f_1$  and  $f_3$  with respect to the state are zero. This yields

$$A_{1,:} = [0 \ 1 \ 0 \ 0 \ 0 \ 0], \quad A_{3,:} = [0 \ 0 \ 0 \ 1 \ 0 \ 0]. \quad (45)$$

**Second row.** The second component  $f_2$  is given in (35). Writing

$$N(\mathbf{x}, u) = u + m_1(g \cos x_3 + l_1 x_4^2) \sin x_3 + m_2(g \cos x_5 + l_2 x_6^2) \sin x_5, \quad (46)$$

one has  $f_2 = N/D$ . At the equilibrium  $(\mathbf{x}_e, u_e)$ ,

$$x_3 = 0, \quad x_4 = 0, \quad x_5 = 0, \quad x_6 = 0, \quad u = 0, \quad (47)$$

and therefore

$$\sin x_3 = \sin x_5 = 0, \quad \cos x_3 = \cos x_5 = 1, \quad D(\mathbf{x}_e) = M. \quad (48)$$

Using the quotient rule and evaluating at the equilibrium gives

$$\frac{\partial f_2}{\partial x_3} \Big|_{(\mathbf{x}_e, u_e)} = \frac{1}{M} \frac{\partial N}{\partial x_3} \Big|_{(\mathbf{x}_e, u_e)} = \frac{1}{M} m_1 g, \quad (49)$$

$$\frac{\partial f_2}{\partial x_5} \Big|_{(\mathbf{x}_e, u_e)} = \frac{1}{M} \frac{\partial N}{\partial x_5} \Big|_{(\mathbf{x}_e, u_e)} = \frac{1}{M} m_2 g, \quad (50)$$

while all other derivatives of  $f_2$  with respect to the state vanish at the equilibrium. Consequently,

$$A_{2,:} = \begin{bmatrix} 0 & 0 & \frac{gm_1}{M} & 0 & \frac{gm_2}{M} & 0 \end{bmatrix}. \quad (51)$$

**Fourth row.** The fourth component is

$$f_4 = -\frac{f_2(\mathbf{x}, u) \cos x_3 + g \sin x_3}{l_1}.$$

Applying the chain rule and evaluating at  $(\mathbf{x}_e, u_e)$ , where  $\sin x_3 = 0$  and  $\cos x_3 = 1$ , yields

$$\begin{aligned} \frac{\partial f_4}{\partial x_3} \Big|_{(\mathbf{x}_e, u_e)} &= -\frac{1}{l_1} \left( \frac{\partial f_2}{\partial x_3} \Big|_{(\mathbf{x}_e, u_e)} \cos x_3 - f_2(\mathbf{x}_e, u_e) \sin x_3 + g \cos x_3 \right) \\ &= -\frac{1}{l_1} \left( \frac{gm_1}{M} + g \right) = -\frac{g(M + m_1)}{Ml_1}, \end{aligned} \quad (52)$$

$$\frac{\partial f_4}{\partial x_5} \Big|_{(\mathbf{x}_e, u_e)} = -\frac{1}{l_1} \frac{\partial f_2}{\partial x_5} \Big|_{(\mathbf{x}_e, u_e)} \cos x_3 = -\frac{gm_2}{Ml_1}, \quad (53)$$

and all remaining partial derivatives of  $f_4$  with respect to the state are zero at the equilibrium. Hence

$$A_{4,:} = \begin{bmatrix} 0 & 0 & -\frac{g(M + m_1)}{Ml_1} & 0 & -\frac{gm_2}{Ml_1} & 0 \end{bmatrix}. \quad (54)$$

**Sixth row.** Similarly, for

$$f_6 = -\frac{f_2(\mathbf{x}, u) \cos x_5 + g \sin x_5}{l_2},$$

the derivatives at  $(\mathbf{x}_e, u_e)$  are

$$\frac{\partial f_6}{\partial x_3} \Big|_{(\mathbf{x}_e, u_e)} = -\frac{1}{l_2} \frac{\partial f_2}{\partial x_3} \Big|_{(\mathbf{x}_e, u_e)} \cos x_5 = -\frac{gm_1}{Ml_2}, \quad (55)$$

$$\frac{\partial f_6}{\partial x_5} \Big|_{(\mathbf{x}_e, u_e)} = -\frac{1}{l_2} \left( \frac{\partial f_2}{\partial x_5} \Big|_{(\mathbf{x}_e, u_e)} \cos x_5 + g \cos x_5 \right) = -\frac{g(M+m_2)}{Ml_2}, \quad (56)$$

with all other partial derivatives of  $f_6$  with respect to the state equal to zero. Thus,

$$A_{6,:} = \begin{bmatrix} 0 & 0 & -\frac{gm_1}{Ml_2} & 0 & -\frac{g(M+m_2)}{Ml_2} & 0 \end{bmatrix}. \quad (57)$$

**Fifth row.** From (38),  $f_5 = x_6$ , so

$$\frac{\partial f_5}{\partial x_6} = 1, \quad (58)$$

and all other derivatives of  $f_5$  with respect to the state are zero:

$$A_{5,:} = [0 \ 0 \ 0 \ 0 \ 0 \ 1]. \quad (59)$$

Collecting all rows, the state Jacobian is

$$A = \begin{bmatrix} 0 & 1 & 0 & 0 & 0 & 0 \\ 0 & 0 & \frac{gm_1}{M} & 0 & \frac{gm_2}{M} & 0 \\ 0 & 0 & 0 & 1 & 0 & 0 \\ 0 & 0 & -\frac{g(M+m_1)}{Ml_1} & 0 & -\frac{gm_2}{Ml_1} & 0 \\ 0 & 0 & 0 & 0 & 0 & 1 \\ 0 & 0 & -\frac{gm_1}{Ml_2} & 0 & -\frac{g(M+m_2)}{Ml_2} & 0 \end{bmatrix}. \quad (60)$$

**Input Jacobian.** The input Jacobian  $B$  is given by

$$B_i = \frac{\partial f_i}{\partial u} \Big|_{(\mathbf{x}_e, u_e)}, \quad i = 1, \dots, 6.$$

From (34), (36), and (38),  $f_1, f_3, f_5$  do not depend on  $u$ , so their derivatives vanish. For  $f_2$ , using  $f_2 = N/D$  and  $D(\mathbf{x}_e) = M$ ,

$$\frac{\partial f_2}{\partial u} \Big|_{(\mathbf{x}_e, u_e)} = \frac{1}{M}. \quad (61)$$

The dependence of  $f_4$  and  $f_6$  on  $u$  arises through  $f_2(\mathbf{x}, u)$ , so

$$\frac{\partial f_4}{\partial u} \Big|_{(\mathbf{x}_e, u_e)} = -\frac{1}{l_1} \frac{\partial f_2}{\partial u} \Big|_{(\mathbf{x}_e, u_e)} \cos x_3 = -\frac{1}{Ml_1}, \quad (62)$$

$$\frac{\partial f_6}{\partial u} \Big|_{(\mathbf{x}_e, u_e)} = -\frac{1}{l_2} \frac{\partial f_2}{\partial u} \Big|_{(\mathbf{x}_e, u_e)} \cos x_5 = -\frac{1}{Ml_2}. \quad (63)$$

Hence

$$B = \begin{bmatrix} 0 \\ 1 \\ \frac{M}{M} \\ 0 \\ -\frac{1}{Ml_1} \\ 0 \\ -\frac{1}{Ml_2} \end{bmatrix}. \quad (64)$$

## 2.4 Linearized State-Space Representation

The linearized dynamics of the double-pendulum crane around the equilibrium  $(\mathbf{x}_e, u_e)$  are thus described by the six-dimensional linear time-invariant system

$$\dot{\mathbf{x}} = A \mathbf{x} + B u, \quad (65)$$

with  $A$  and  $B$  given above. This model provides a first-order approximation of the original nonlinear dynamics for small deviations around the hanging configuration and will be used as the basis for the controller and observer design in the remaining components of the project.

## 3 First Component, Part C: Controllability of the Linearized System

The linearized dynamics around the hanging equilibrium are given by

$$\dot{\mathbf{x}} = A \mathbf{x} + B u, \quad (66)$$

with  $A \in \mathbb{R}^{6 \times 6}$  and  $B \in \mathbb{R}^{6 \times 1}$  as derived in Part B. To assess controllability, the standard controllability matrix

$$\mathcal{C} = [B \ AB \ A^2B \ A^3B \ A^4B \ A^5B] \in \mathbb{R}^{6 \times 6} \quad (67)$$

is formed. The linearized system is controllable if and only if  $\text{rank}(\mathcal{C}) = 6$ , or equivalently  $\det(\mathcal{C}) \neq 0$ .

Because of the symbolic dependence on the physical parameters  $M, m_1, m_2, l_1, l_2$  and  $g$ , the entries of  $\mathcal{C}$  are cumbersome to write explicitly. Instead, the matrix powers  $A^k B$ ,  $k = 0, \dots, 5$ , and the determinant of  $\mathcal{C}$  were computed symbolically using Python and a computer algebra package (SymPy). The corresponding implementation is provided in the file `src/component1_C.py`. After simplification and factorization, the determinant takes the form

$$\det(\mathcal{C}) = -\frac{g^6 (l_1 - l_2)^2}{M^6 l_1^6 l_2^6}. \quad (68)$$

The controllability condition  $\det(\mathcal{C}) \neq 0$  therefore reduces to

$$M \neq 0, \quad l_1 \neq 0, \quad l_2 \neq 0, \quad l_1 \neq l_2, \quad g \neq 0. \quad (69)$$

Notably, the masses  $m_1$  and  $m_2$  cancel out of the determinant and thus do not affect controllability of the linearized model.

For a physically meaningful crane,

$$M > 0, \quad m_1 > 0, \quad m_2 > 0, \quad l_1 > 0, \quad l_2 > 0, \quad g > 0, \quad (70)$$

these conditions reduce to requiring that the two link lengths are distinct:

$$l_1 \neq l_2. \quad (71)$$

Under this assumption, the controllability matrix  $\mathcal{C}$  has full rank 6, and the linearized double-pendulum crane system is controllable around the hanging equilibrium.

## 4 LQR Design and Closed-Loop Stability Analysis

For the numerical values

$$M = 1000 \text{ kg}, \quad m_1 = m_2 = 100 \text{ kg}, \quad l_1 = 20 \text{ m}, \quad l_2 = 10 \text{ m},$$

the linearized model obtained in Part B at the hanging-down equilibrium  $\bar{x} = 0, \bar{u} = 0$  takes the form

$$\dot{\mathbf{x}} = Ax + Bu,$$

with

$$A = \begin{bmatrix} 0 & 1 & 0 & 0 & 0 & 0 \\ 0 & 0 & 0.981 & 0 & 0.981 & 0 \\ 0 & 0 & 0 & 1 & 0 & 0 \\ 0 & 0 & -0.53955 & 0 & -0.04905 & 0 \\ 0 & 0 & 0 & 0 & 0 & 1 \\ 0 & 0 & -0.09810 & 0 & -1.07910 & 0 \end{bmatrix}, \quad B = \begin{bmatrix} 0 \\ 10^{-3} \\ 0 \\ -5 \times 10^{-5} \\ 0 \\ -10^{-4} \end{bmatrix}. \quad (72)$$

## 4.1 Controllability check

The controllability matrix of the linearized system is

$$\mathcal{C} = [B, AB, A^2B, A^3B, A^4B, A^5B] \in \mathbb{R}^{6 \times 6}.$$

Using the numerical matrices in (72), the rank test yields

$$(\mathcal{C}) = 6.$$

Since the state dimension is  $n = 6$ , the pair  $(A, B)$  is controllable for the chosen parameter values, in agreement with the general condition derived in Part C (which requires in particular  $l_1 \neq l_2$ ). No uncontrollable modes are present at the hanging-down equilibrium.

## 4.2 LQR controller design and grid search over $Q, R$

To design a state-feedback controller we consider the continuous-time LQR problem with cost

$$J = \int_0^\infty (x(t)^\top Q x(t) + u(t)^\top R u(t)) dt.$$

Several diagonal choices of  $Q$  and scalar values of  $R$  were tested in order to balance tracking performance and actuator effort. For each candidate pair  $(Q, R)$ , the algebraic Riccati equation

$$A^\top P + PA - PBR^{-1}B^\top P + Q = 0$$

was solved numerically, the corresponding gain

$$K = R^{-1}B^\top P$$

was computed, and the closed-loop eigenvalues of

$$A_{\text{cl}} = A - BK$$

were evaluated. The main performance indicators (settling time of the cart position, maximum pendulum angles, maximum control force and  $\max \Re\{\lambda(A_{\text{cl}})\}$ ) are summarized in Figure 1.

Design	$Q_{\text{diag}}$	$R$	$ts\_x\_lin$ [s]	$ts\_x\_non$ [s]	$\max 01 _{\text{lin}}$ [deg]	$\max 01 _{\text{non}}$ [deg]	$\max 02 _{\text{lin}}$ [deg]	$\max 02 _{\text{non}}$ [deg]	$\max u _{\text{lin}}$ [N]	$\max u _{\text{non}}$ [N]	$\max \Re\{\lambda_{\text{cl}}\}$
1	[1. 0.1 10. 0.5 10. 0.5]	0.001	40.0	40.0	5.473139043880454	5.47289913406012	5.0	5.0	17.579027675039793	17.513054023953526	-0.0031606584426297803
2	[1. 0.1 10. 0.5 10. 0.5]	0.01	40.0	40.0	5.629027496740284	5.628580747620892	5.0	5.0	6.275437725773117	6.262063700999841	-0.00100051664491976
3	[1. 0.1 10. 0.5 10. 0.5]	0.1	40.0	40.0	5.675547003990321	5.6751380246246015	5.0	5.0	2.4594751946909326	2.4581689630500994	-0.003164237071525074
4	[10. 0.1 50. 1. 50. 1.]	0.001	40.0	40.0	5.147876475280753	5.14798275004017	5.0	5.0	52.27728103969156	52.27728103969156	-0.007526923879398073
5	[10. 0.1 50. 1. 50. 1.]	0.01	40.0	40.0	5.5069934326945935	5.506674824931448	5.0	5.0	17.036930563561956	17.036930563561956	-0.002403829795096721
6	[10. 0.1 50. 1. 50. 1.]	0.1	40.0	40.0	5.640478510525309	5.64009857173303	5.0	5.0	5.59183559572134	5.571620501140285	-0.0007609098230936711
7	[1. 0.1 100. 1. 100. 1.]	0.001	40.0	40.0	5.232820556977738	5.232555488123564	5.0	5.0	44.7320540569969	44.702310465476984	-0.009011116854225391
8	[1. 0.1 100. 1. 100. 1.]	0.01	40.0	40.0	5.542735886738803	5.542432115437358	5.0	5.0	16.16101407163132	16.160763816037353	-0.0028567239452445357
9	[1. 0.1 100. 1. 100. 1.]	0.1	40.0	40.0	5.647192558808729	5.6468635653577415	5.0	5.0	5.805570059780463	5.804826030246499	-0.0009036032314180499

**Figure 1:** Summary of the LQR design candidates obtained from a grid search over diagonal  $Q$  and scalar  $R$ . Each row reports the closed-loop eigenvalues and several performance measures for the linear and nonlinear simulations.

Among all candidates, Design #2

$$Q = \text{diag}(1, 0.1, 10, 0.5, 10, 0.5), \quad R = 0.01,$$

was selected for the following reasons:

- All closed-loop eigenvalues lie in the open left half-plane with  $\max \Re\{\lambda(A_{\text{cl}})\} \approx -10^{-3}$ , providing asymptotic stability with a moderate convergence rate.
- The maximum control effort in the nonlinear simulation is  $|u(t)|_{\max} \approx 6.3$  N, which is significantly smaller than for more aggressive designs (e.g. Design #1, #4, #7), while still keeping the response well damped.
- The peak pendulum angles for Design #2 remain close to those of the other designs (around  $5^\circ$ – $6^\circ$ ), so reducing the control effort does not noticeably degrade the state response.

Overall, Design #2 provides a good compromise between stabilization speed and control amplitude, and it will be used in the subsequent simulations and stability analysis.

### 4.3 Closed-loop simulations: linear vs. nonlinear model

The feedback law

$$u = -Kx$$

obtained from Design #2 was first applied to the linearized model, resulting in the closed-loop dynamics

$$\dot{x} = (A - BK)x.$$

The same state feedback was then applied to the original nonlinear model  $\dot{x} = f(x, u)$  with

$$u = -Kx,$$

using the exact nonlinear expressions derived in Part A. Both systems were simulated from the same initial condition

$$x(0) = [0.5 \ 0 \ 5^\circ \ 0 \ -5^\circ \ 0]^\top,$$

where  $5^\circ$  is converted to radians in the implementation.

Figures 2–5 show the comparison between the linear and nonlinear responses under the selected LQR controller.

The cart position trajectories in Figure 2 show that the linearized model provides an accurate approximation of the nonlinear response around the equilibrium: both signals almost overlap over the entire simulation horizon. The pendulum angles in Figures 3–4 exhibit small oscillations with peak values below approximately  $6^\circ$ , again with very similar behaviour for the linear and nonlinear systems. The control input depicted in Figure 5 confirms that the maximum actuation level remains close to 6 N for the nonlinear model, consistent with the summary reported in Figure 1.

### 4.4 Lyapunov indirect method

The closed-loop nonlinear system with state feedback  $u = -Kx$  can be written as

$$\dot{x} = f_{\text{cl}}(x) := f(x, -Kx),$$

where  $f(x, u)$  denotes the original nonlinear dynamics in state-space form. The equilibrium at the hanging-down configuration satisfies

$$x = 0, \quad u = 0, \quad f_{\text{cl}}(0) = 0.$$

Linearizing  $f_{\text{cl}}(x)$  around  $x = 0$  gives

$$\dot{x} = \left. \frac{\partial f_{\text{cl}}}{\partial x} \right|_{x=0} x = (A - BK)x = A_{\text{cl}}x.$$

For Design #2, the eigenvalues of  $A_{\text{cl}}$  are

$$\lambda(A_{\text{cl}}) \approx \{-0.0645 \pm j 0.0646, -0.00176 \pm j 1.0430, -0.00100 \pm j 0.7285\},$$

so that all eigenvalues lie strictly in the open left half-plane and  $\max \Re\{\lambda(A_{\text{cl}})\} \approx -10^{-3} < 0$ .

By Lyapunov's indirect (linearization) method, if all eigenvalues of the Jacobian at an equilibrium have strictly negative real parts, then the equilibrium of the nonlinear system is locally asymptotically stable. Since all eigenvalues of  $A_{\text{cl}}$  have negative real part, the hanging-down equilibrium of the nonlinear crane with the chosen LQR state feedback is *locally asymptotically stable*.

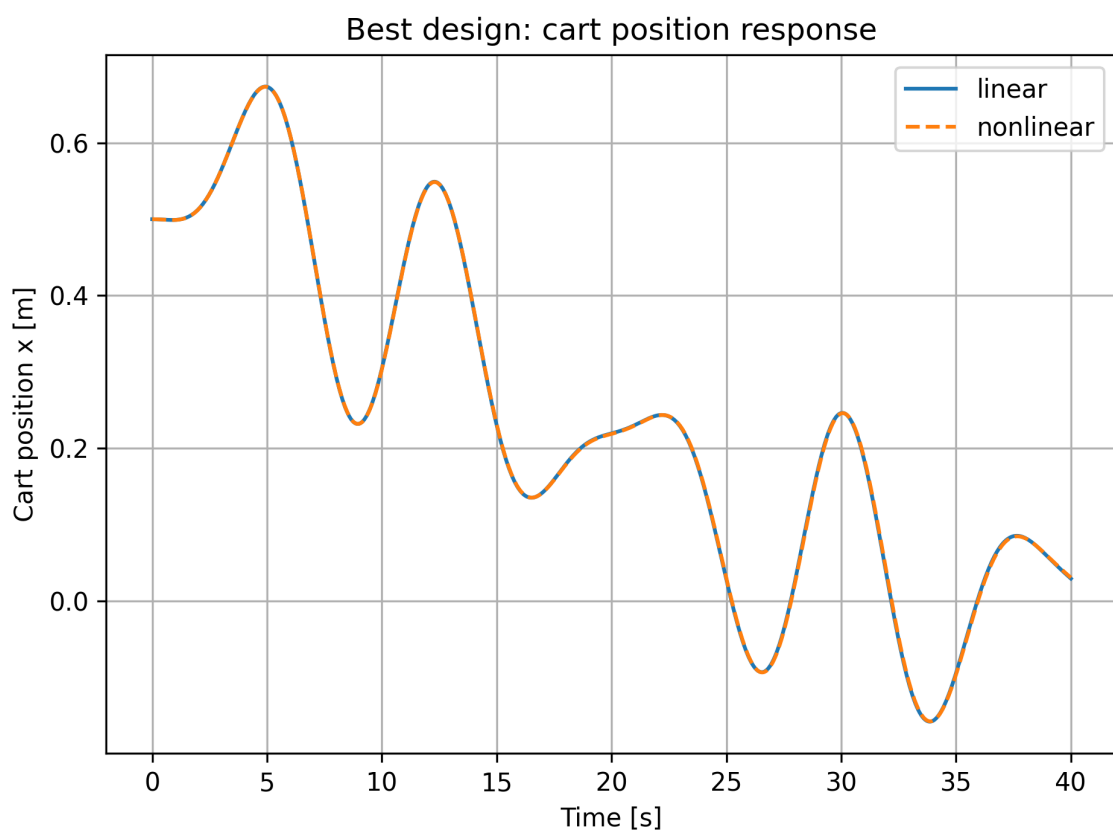


**Figure 2:** Cart position response for the selected LQR design (Design #2), comparing the linearized model and the original nonlinear model.

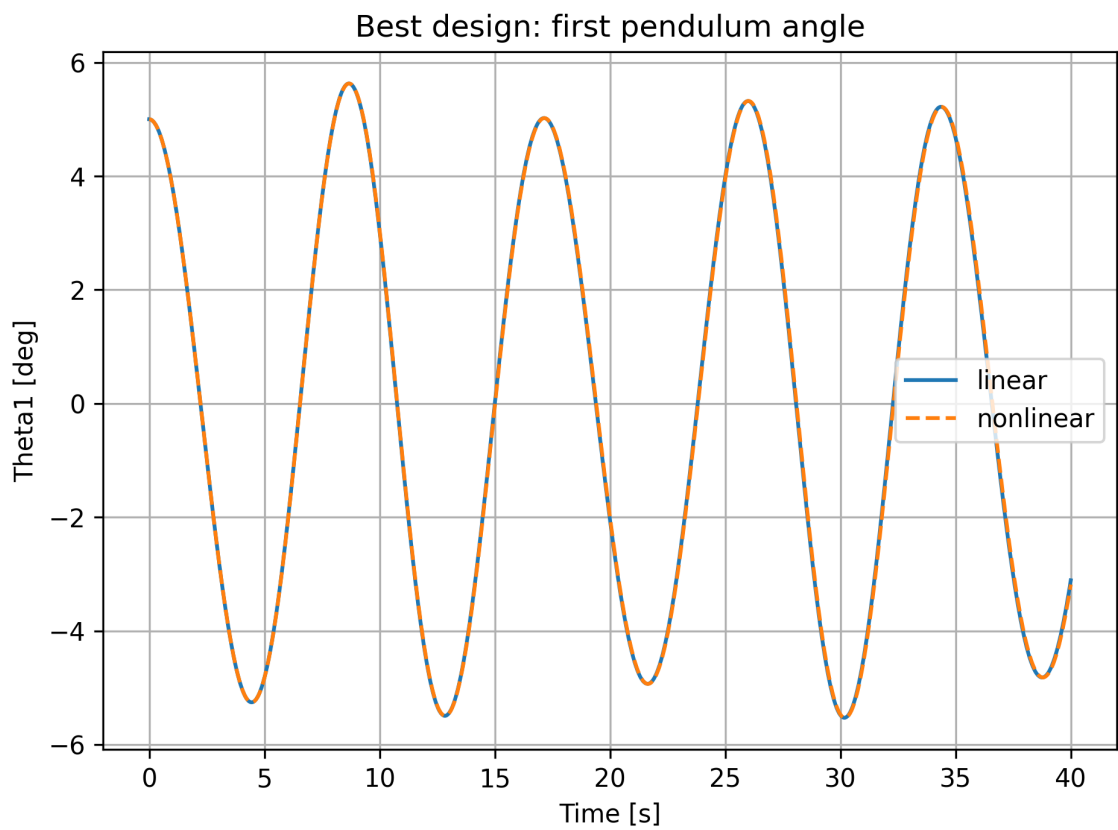


**Figure 3:** First pendulum angle  $\theta_1(t)$  for the selected LQR design, linear vs. nonlinear model.

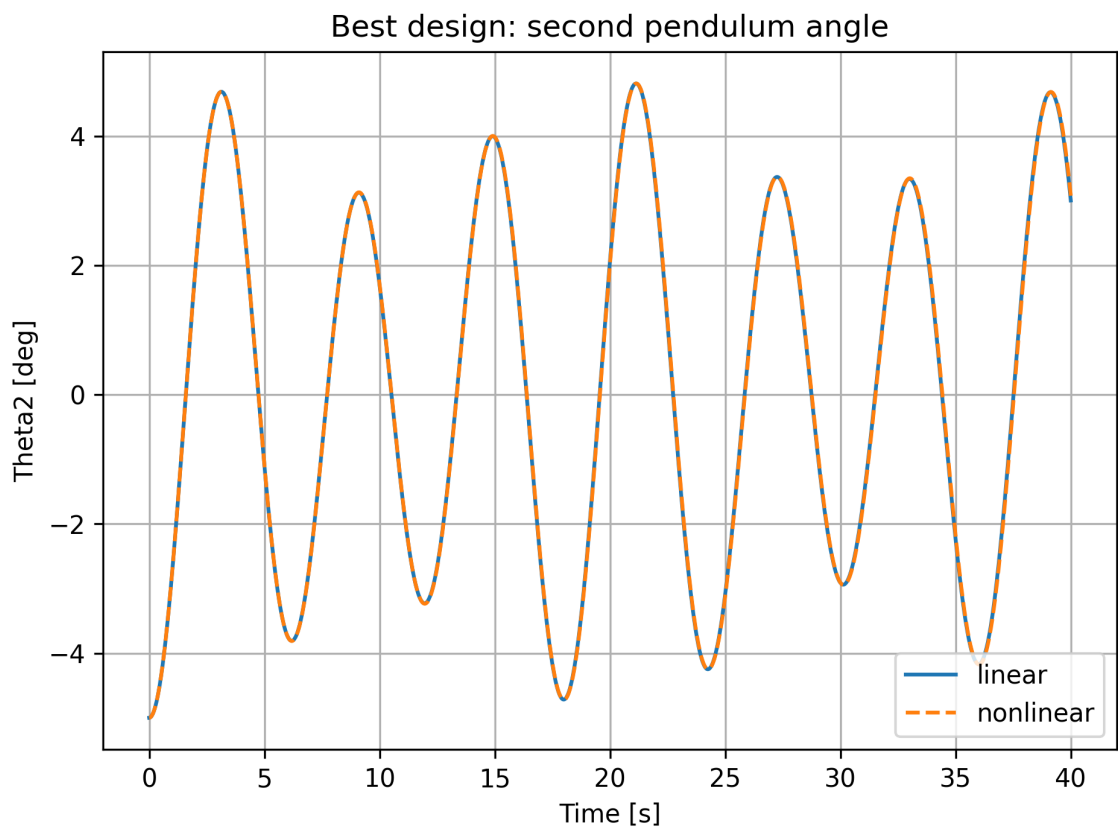


**Figure 4:** Second pendulum angle  $\theta_2(t)$  for the selected LQR design, linear vs. nonlinear model.

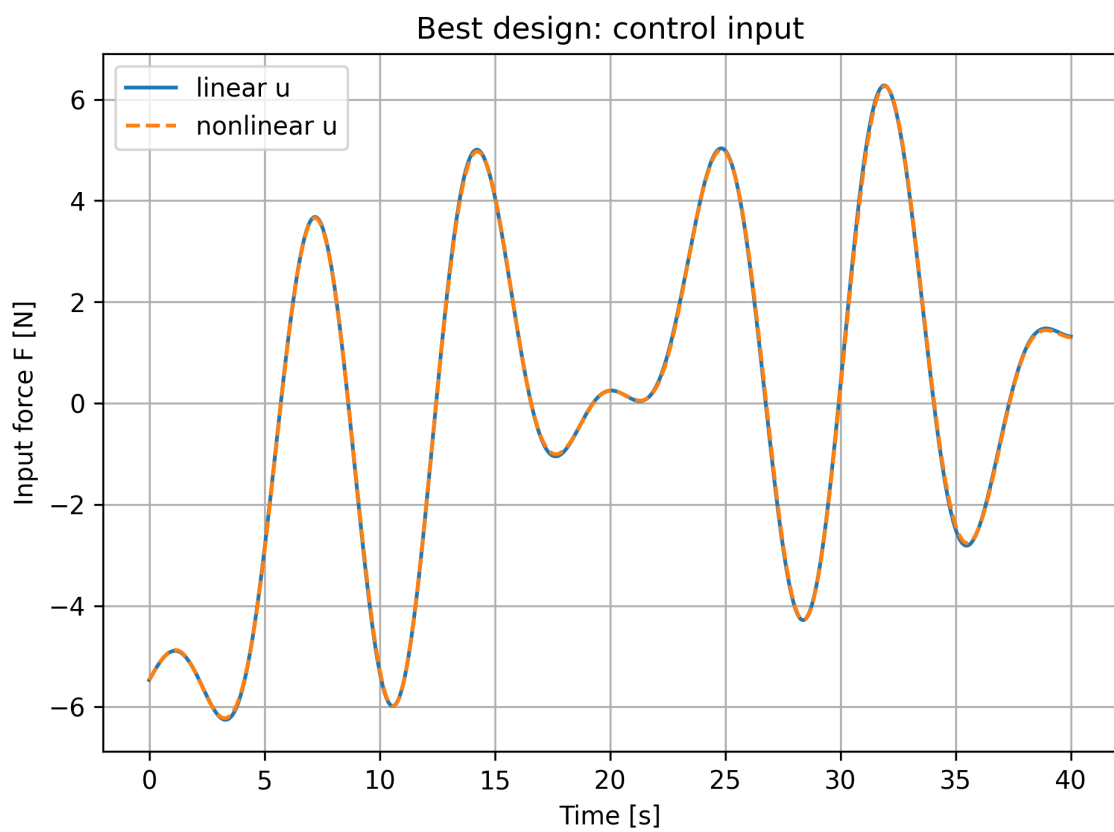


**Figure 5:** Control input  $u(t)$  for the selected LQR design, linear vs. nonlinear model.

## 5 Component 2E: Observability for Different Output Selections

For the linearized model obtained in Component 2,

$$\dot{x}(t) = Ax(t) + Bu(t), \quad y(t) = Cx(t),$$

the state vector is

$$x = [x \ \dot{x} \ \theta_1 \ \dot{\theta}_1 \ \theta_2 \ \dot{\theta}_2]^\top \in \mathbb{R}^6.$$

In this component, the goal is to assess observability of the linearized system for several possible output selections, assuming that the system matrices  $A, B$  are fixed as in Component 2.

### 5.1 Method: duality between observability and controllability

For a linear time-invariant system  $(A, C)$ , observability can be tested via the duality relation

$$(A, C) \text{ observable} \iff (A^\top, C^\top) \text{ controllable.}$$

Instead of forming the observability matrix for  $(A, C)$ , the analysis proceeds by constructing the controllability matrix for the dual pair  $(A^\top, C^\top)$ ,

$$\mathcal{C}_{\text{dual}} = [C^\top, A^\top C^\top, (A^\top)^2 C^\top, \dots, (A^\top)^5 C^\top] \in \mathbb{R}^{6 \times 6},$$

and checking its rank. Since the state dimension is  $n = 6$ , the condition

$$(\mathcal{C}_{\text{dual}}) = 6$$

is equivalent to full observability of the original pair  $(A, C)$ .

All symbolic and numeric rank computations were carried out in Python using `sympy`. The corresponding script is provided in `src/component2_E.observability.py`.

### 5.2 Output choices and associated $C$ matrices

The problem statement specifies four candidate output vectors:

$$y(t) = x(t), \quad y(t) = [\theta_1(t) \ \theta_2(t)], \quad y(t) = [x(t) \ \theta_2(t)], \quad y(t) = [x(t) \ \theta_1(t) \ \theta_2(t)].$$

These choices correspond to the following  $C$  matrices:

$$\text{Case 1: } y = x \Rightarrow C_1 = [1 \ 0 \ 0 \ 0 \ 0 \ 0], \quad (73)$$

$$\text{Case 2: } y = (\theta_1, \theta_2) \Rightarrow C_2 = [0 \ 0 \ 1 \ 0 \ 0 \ 0], \quad (74)$$

$$\text{Case 3: } y = (x, \theta_2) \Rightarrow C_3 = [1 \ 0 \ 0 \ 0 \ 0 \ 0], \quad (75)$$

$$\text{Case 4: } y = (x, \theta_1, \theta_2) \Rightarrow C_4 = [1 \ 0 \ 0 \ 0 \ 0 \ 0]. \quad (76)$$

### 5.3 Rank test via $(A^\top, C^\top)$

For each output choice, the controllability matrix of the dual pair  $(A^\top, C_i^\top)$  was constructed and its rank evaluated symbolically. The results are:

- Case 1:  $y = x$ ,

$$(\mathcal{C}_{\text{dual}}(A^\top, C_1^\top)) = 6,$$

hence  $(A, C_1)$  is observable.

- Case 2:  $y = (\theta_1, \theta_2)$ ,  
 $(\mathcal{C}_{\text{dual}}(A^\top, C_2^\top)) = 4$ ,  
hence  $(A, C_2)$  is *not* observable.

- Case 3:  $y = (x, \theta_2)$ ,  
 $(\mathcal{C}_{\text{dual}}(A^\top, C_3^\top)) = 6$ ,  
hence  $(A, C_3)$  is observable.
- Case 4:  $y = (x, \theta_1, \theta_2)$ ,  
 $(\mathcal{C}_{\text{dual}}(A^\top, C_4^\top)) = 6$ ,  
hence  $(A, C_4)$  is observable.

To confirm that these conclusions are not an artifact of symbolic simplification, a numerical check was also performed by substituting the parameter values

$$M = 1000 \text{ kg}, \quad m_1 = m_2 = 100 \text{ kg}, \quad l_1 = 20 \text{ m}, \quad l_2 = 10 \text{ m}, \quad g = 9.81 \text{ m/s}^2.$$

In all cases, the numerical ranks coincide with the symbolic ones:

$$\begin{aligned} (\mathcal{C}_{\text{dual}}(A^\top, C_1^\top)) &= 6, \\ (\mathcal{C}_{\text{dual}}(A^\top, C_2^\top)) &= 4, \\ (\mathcal{C}_{\text{dual}}(A^\top, C_3^\top)) &= 6, \\ (\mathcal{C}_{\text{dual}}(A^\top, C_4^\top)) &= 6. \end{aligned}$$

## 5.4 Discussion

The observability analysis shows that the linearized crane system is observable when the cart position  $x(t)$  is included among the measured outputs, i.e. for the choices

$$y = x, \quad y = (x, \theta_2), \quad y = (x, \theta_1, \theta_2).$$

In contrast, when only the two link angles  $(\theta_1, \theta_2)$  are measured, the observability rank drops to  $4 < 6$ , and two state directions remain unobservable. In that case, it is not possible to reconstruct the full six-dimensional state vector from the output history, and no full-order observer can be designed to estimate all states. Conversely, any of the output configurations that include the cart position  $x$  guarantees full observability of the linearized model and is suitable for designing a Luenberger

## Component 2F – Luenberger observer design and comparison

In Component 2E we showed that the linearized cart–double–pendulum system is observable for the following output choices:

$$y_1 = x, \quad y_2 = \begin{bmatrix} x \\ \theta_2 \end{bmatrix}, \quad y_3 = \begin{bmatrix} x \\ \theta_1 \\ \theta_2 \end{bmatrix}.$$

In this section we design a Luenberger observer for each observable output and compare their performance on both the linearized model and the original nonlinear dynamics.

### Observer structure and separation principle

The plant with state feedback is

$$\begin{aligned} \dot{x}(t) &= Ax(t) + Bu(t), \\ y(t) &= Cx(t), \\ u(t) &= -Kx(t) + r(t), \end{aligned}$$

where the gain  $K$  is the LQR gain obtained in Component 1D using

$$Q = \text{diag}(1, 0.1, 10, 0.5, 10, 0.5), \quad R = 0.01,$$

which gave the closed-loop eigenvalues

$$\lambda_{\text{cl}}(A - BK) = \{-0.0645 \pm j0.0646, -0.00176 \pm j1.0430, -0.00100 \pm j0.7285\}.$$

Since in practice we do not have access to the full state  $x(t)$ , we build a Luenberger observer,

$$\begin{aligned}\dot{\hat{x}}(t) &= A\hat{x}(t) + Bu(t) + L(y(t) - C\hat{x}(t)), \\ u(t) &= -K\hat{x}(t) + r(t),\end{aligned}$$

and use  $\hat{x}(t)$  instead of the true state in the feedback law. The estimation error  $\tilde{x}(t) = x(t) - \hat{x}(t)$  satisfies

$$\dot{\tilde{x}}(t) = (A - LC)\tilde{x}(t),$$

so the error dynamics are asymptotically stable if all eigenvalues of  $A - LC$  lie in the open left half-plane.

By the separation principle the closed-loop eigenvalues of the combined controller–observer system are given by the union of  $\sigma(A - BK)$  and  $\sigma(A - LC)$ . Therefore the state-feedback gain  $K$  designed in Component 1D can be kept fixed, and we are free to choose  $L$  to shape the observer poles without destroying the stability of the state-feedback loop.

## Pole-placement strategy and speed factor

For each output matrix  $C$  we design  $L$  by pole placement using the dual system  $(A^\top, C^\top)$ . Let  $\lambda_i^{\text{cl}} \in \sigma(A - BK)$  denote the LQR closed-loop poles above. We introduce a *speed factor*  $\alpha > 0$  and define desired observer poles as

$$\lambda_i^{\text{obs}}(\alpha) = \alpha \Re(\lambda_i^{\text{cl}}) + j \Im(\lambda_i^{\text{cl}}), \quad i = 1, \dots, 6.$$

Thus increasing  $\alpha$  moves the observer poles further to the left, making the estimation error converge faster while keeping the oscillation frequencies similar to the plant.

For each output choice  $C \in \{C_{y_1}, C_{y_2}, C_{y_3}\}$  we consider the set of speed factors

$$\alpha \in \{4, 8, 12, 20\},$$

and compute the corresponding observer gain by

$$L(\alpha) = \text{place}(A^\top, C^\top, \{\lambda_i^{\text{obs}}(\alpha)\}_{i=1}^6)^\top.$$

As a reference, we also simulate a “no-observer” case  $\alpha = 0 \Rightarrow L = 0$ , where the dynamics of the estimation error are  $\dot{\tilde{x}} = A\tilde{x}$  and therefore unstable for the linearized system.

The resulting eigenvalues of  $A - LC$  for several outputs and speed factors are, e.g. for  $y = x$ ,

$$\lambda(A - LC) = \{-0.2579 \pm j0.0646, -0.00703 \pm j1.0430, -0.00400 \pm j0.7285\} \quad (\alpha = 4),$$

$$\lambda(A - LC) = \{-1.2899 \pm j0.0646, -0.0352 \pm j1.0430, -0.0200 \pm j0.7285\} \quad (\alpha = 20),$$

confirming that the real parts are approximately scaled by  $\alpha$  relative to the LQR poles.

## Simulation setup

For each output choice and each speed factor  $\alpha$  we simulate

- the **linearized** plant with the Luenberger observer, and
- the **nonlinear** cart–double–pendulum model with the same controller  $u(t) = -K\hat{x}(t) + r(t)$  and the same observer dynamics.

The simulations use the same initial condition as in Component 1D, with a nonzero cart displacement and small initial pendulum angles, and a unit step reference  $r(t)$  acting on the cart position channel. For each run we record:

- the state estimation error  $e(t) = x(t) - \hat{x}(t)$ ,
- the control input  $u(t)$ , and
- the output  $y(t)$ .

To compare designs we compute the following performance indices on the *nonlinear* simulations:

$$\begin{aligned} \text{ISE}_{\text{non}} &= \int_0^T \|e(t)\|_2^2 dt, \\ \text{max\_err\_x\_non} &= \max_{t \in [0, T]} |x(t) - \hat{x}(t)|, \\ \text{max\_err\_}\theta_1,\theta_2\text{\_non} &= \max_{t \in [0, T]} |\theta_{1,2}(t) - \hat{\theta}_{1,2}(t)|, \\ \text{max\_u\_non} &= \max_{t \in [0, T]} |u(t)|. \end{aligned}$$

Analogous indices  $\text{ISE}_{\text{lin}}$  are computed on the linear simulations. All metrics are summarized in the comparison table (Fig. 6).

## Quantitative comparison of observers

Table 6 reports the nonlinear ISE and the maximum estimation errors and control input for all outputs and speed factors considered. The main trends are:

- For each output, increasing the speed factor  $\alpha$  from 4 to 20 consistently *reduces* the nonlinear estimation ISE. For example, for  $y = x$

$$\text{ISE}_{\text{non}} : 1.348 (\alpha = 4) \rightarrow 0.950 (\alpha = 8) \rightarrow 0.726 (\alpha = 12) \rightarrow 0.509 (\alpha = 20).$$

- The maximum estimation errors of the pendulum angles also decrease with  $\alpha$ . For the output  $y = (x, \theta_2)$  we observe  $\text{max\_err\_}\theta_2\text{\_non}$  dropping from 0.173 rad at  $\alpha = 4$  to 0.087 rad at  $\alpha = 20$ .
- Faster observers demand larger control effort. For  $y = (x, \theta_1, \theta_2)$  the peak control amplitude increases from about 38 N at  $\alpha = 4$  to approximately 63.8 N at  $\alpha = 20$ .
- The “no-observer” case ( $\alpha = 0$ ) behaves poorly: the ISE is much larger and the estimation error does not decay, confirming that a dedicated observer is needed for this linearization.

Based on these metrics, and because the assignment asks for the “best” observer, we select the design with  $\alpha = 20$  for all observable outputs. This choice gives the smallest nonlinear ISE and noticeably tighter tracking of the true states, at the cost of higher but still reasonable control effort.

## Time-domain behaviour of the best observers

Figures 7–12 show the time histories for the best observers with  $\alpha = 20$  for each output choice, for both the linearized and nonlinear plants.

**Case  $y = x$ .** Figures 7 and 8 compare the cart position and pendulum angles for the linear and nonlinear models. The estimated cart position  $\hat{x}$  is almost indistinguishable from the true position, and the pendulum angles are reconstructed with small phase and amplitude errors. The observer quickly rejects the initial state mismatch, and the estimation error remains bounded and small while the controller tracks the reference.

output	speed factor	ISE lin	ISE non	max_err_x_non	max_err_theta1_non	max_err_theta2_non	max_u_non
$y = x$	4.0	1.3497719266892512	1.34845436182962668	0.5	0.09601374669321382	0.08726646259971647	10.365536081726095
$y = x$	8.0	0.9500710381557895	0.9492424367095951	0.5	0.09427575683122496	0.08726646259971647	15.4659418872391
$y = x$	12.0	0.7256908555479269	0.7251863476439073	0.5	0.09519434512788362	0.08726646259971647	22.77817844922014
$y = x$	20.0	0.5088734236716115	0.5087549276245571	0.5	0.09700193924258146	0.08843978352717866	37.570902550112635
$y = x$	0.0	6.6828955510271895	6.680918558976495	0.7027527257110673	0.09985724321039319	0.08726646259971647	2.7549442217324698
$y = (x, \theta_2)$	4.0	2.771927004717157	2.7710274650501425	0.5	0.11299420142240306	0.1732562706556658	30.238506245397478
$y = (x, \theta_2)$	8.0	2.213948859397911	2.211012269612136	0.5	0.12115296008359629	0.14402000981560545	41.12413951182405
$y = (x, \theta_2)$	12.0	1.820942426022814	1.8169210649458916	0.5	0.12237320381500062	0.11615155422420927	47.7503500447763
$y = (x, \theta_2)$	20.0	1.325613634939127	1.3216939532938417	0.5	0.1493523369823568	0.08726646259971647	54.54495753736488
$y = (x, \theta_2)$	0.0	3.66407768583497	3.6645380846727	0.5076134182205286	0.11454548682832628	0.19301671940766843	12.997539650907347
$y = (x, \theta_1, \theta_2)$	4.0	7.282912952993655	7.287337801125633	0.5	0.30391921043731857	0.4722630555800163	38.07382206030201
$y = (x, \theta_1, \theta_2)$	8.0	5.896679590130804	5.891538063149691	0.5	0.2814040493436054	0.39514515848396675	50.264849176929374
$y = (x, \theta_1, \theta_2)$	12.0	4.6920451916729995	4.688392399491078	0.5	0.23046414934231604	0.36908086573710963	54.01331459971655
$y = (x, \theta_1, \theta_2)$	20.0	3.423855140892173	3.430614836667776	0.5	0.18699335763112213	0.28452049638410926	63.83010805961389
$y = (x, \theta_1, \theta_2)$	0.0	8.653414655491302	8.682283158543038	0.5	0.4918056925790857	0.41824183389413006	69.54453026205633

**Figure 6:** Performance summary for all Luenberger observers in Component 2F. For each observable output  $y$  and speed factor  $\alpha$ , the table lists the integral squared estimation error (ISE) for the linear and nonlinear models, the maximum estimation errors in cart position and pendulum angles, and the maximum control input. The best design for each output (minimum nonlinear ISE) occurs at  $\alpha = 20$ .

**Case  $y = (x, \theta_2)$ .** In Figures 9 and 10 the observer uses measurements of the cart position and the second pendulum angle. Even though  $\theta_1$  is not directly measured, the observer reconstructs it accurately. Compared with the  $y = x$  case, the extra information on  $\theta_2$  allows the observer to use a slightly larger control action but yields smaller angle estimation errors, consistent with the ISE values in the comparison table.

**Case  $y = (x, \theta_1, \theta_2)$ .** Finally, Figures 11 and 12 show the case where all three coordinates  $x, \theta_1, \theta_2$  are measured. As expected, the observer is able to match the measured angles very closely, and the remaining unmeasured states (velocities) are also reconstructed well. This design has the smallest ISE among the three outputs, but it also requires the largest control effort, as reflected in the peak value of  $u(t)$ .

Overall, the experiments confirm the expected trade-off: making the observer poles faster (larger speed factor) improves state reconstruction and reduces the integral squared estimation error, but increases the required control effort. In this project we therefore adopt  $\alpha = 20$  as the “best” Luenberger observer design for each observable output, since it provides very accurate state estimates for both the linearized and nonlinear models while keeping the control input within a reasonable range.

## Component 2G – LQG output feedback (smallest output vector) and nonlinear simulation

In this component we design an *output feedback* controller using the LQG method. Among the observable output choices from Component 2E, we choose the smallest output vector that still provides good performance:

$$y(t) = \begin{bmatrix} x(t) \\ \theta_1(t) \\ \theta_2(t) \end{bmatrix}.$$

The LQG controller is then applied to (i) the linearized plant and (ii) the original nonlinear cart–double-pendulum dynamics. All simulation figures referenced below are included in the submission.

### Linearized model and chosen output

We use the linearized state-space model around the upright equilibrium,

$$\begin{aligned} \dot{x}(t) &= Ax(t) + Bu(t), \\ y(t) &= Cx(t), \end{aligned}$$

with state

$$x = [x \quad \dot{x} \quad \theta_1 \quad \dot{\theta}_1 \quad \theta_2 \quad \dot{\theta}_2]^\top,$$

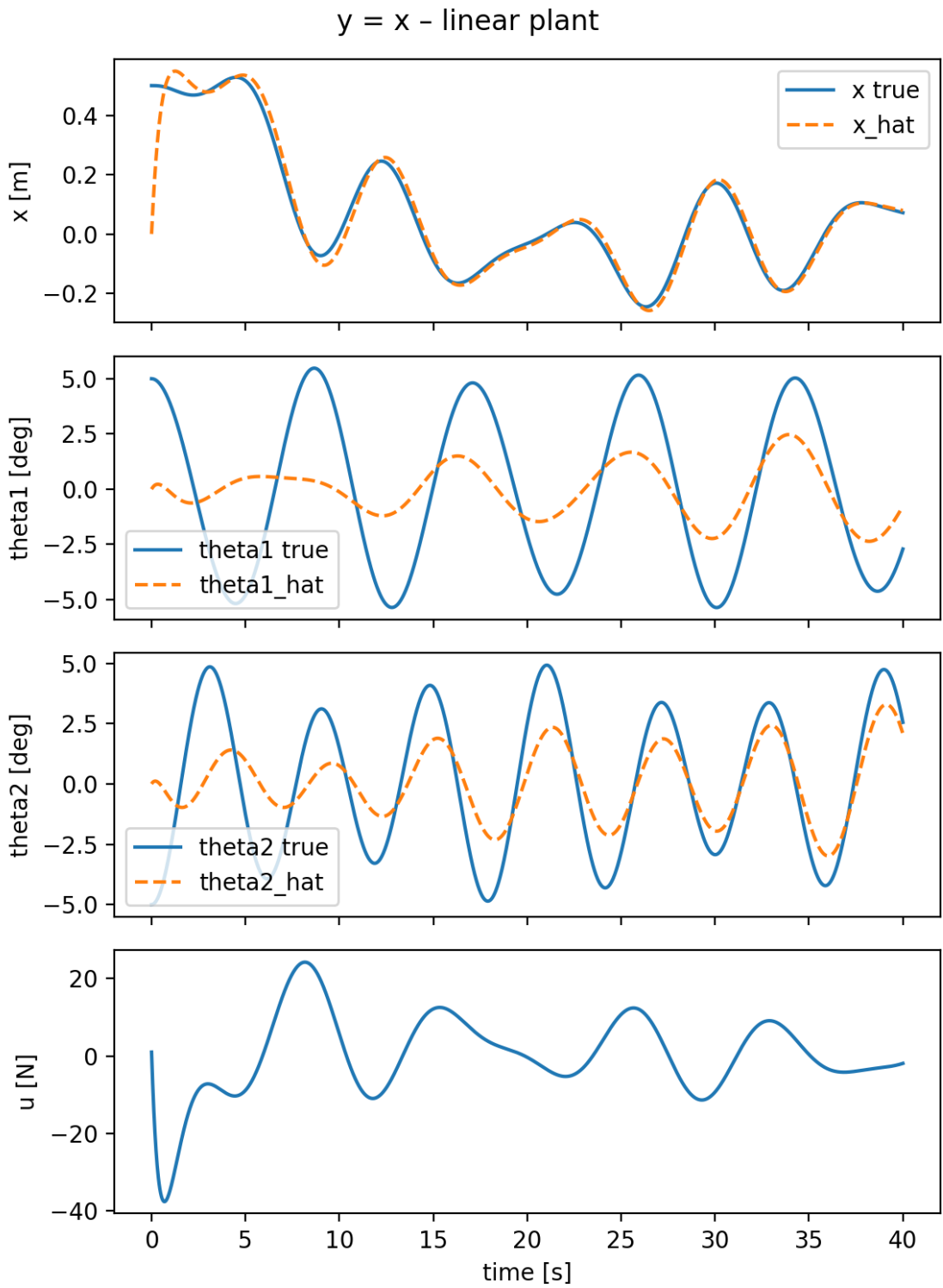


**Figure 7:** Best observer for output  $y = x$  (speed factor  $\alpha = 20$ ), linearized plant. Solid lines: true states; dashed lines: observer estimates.

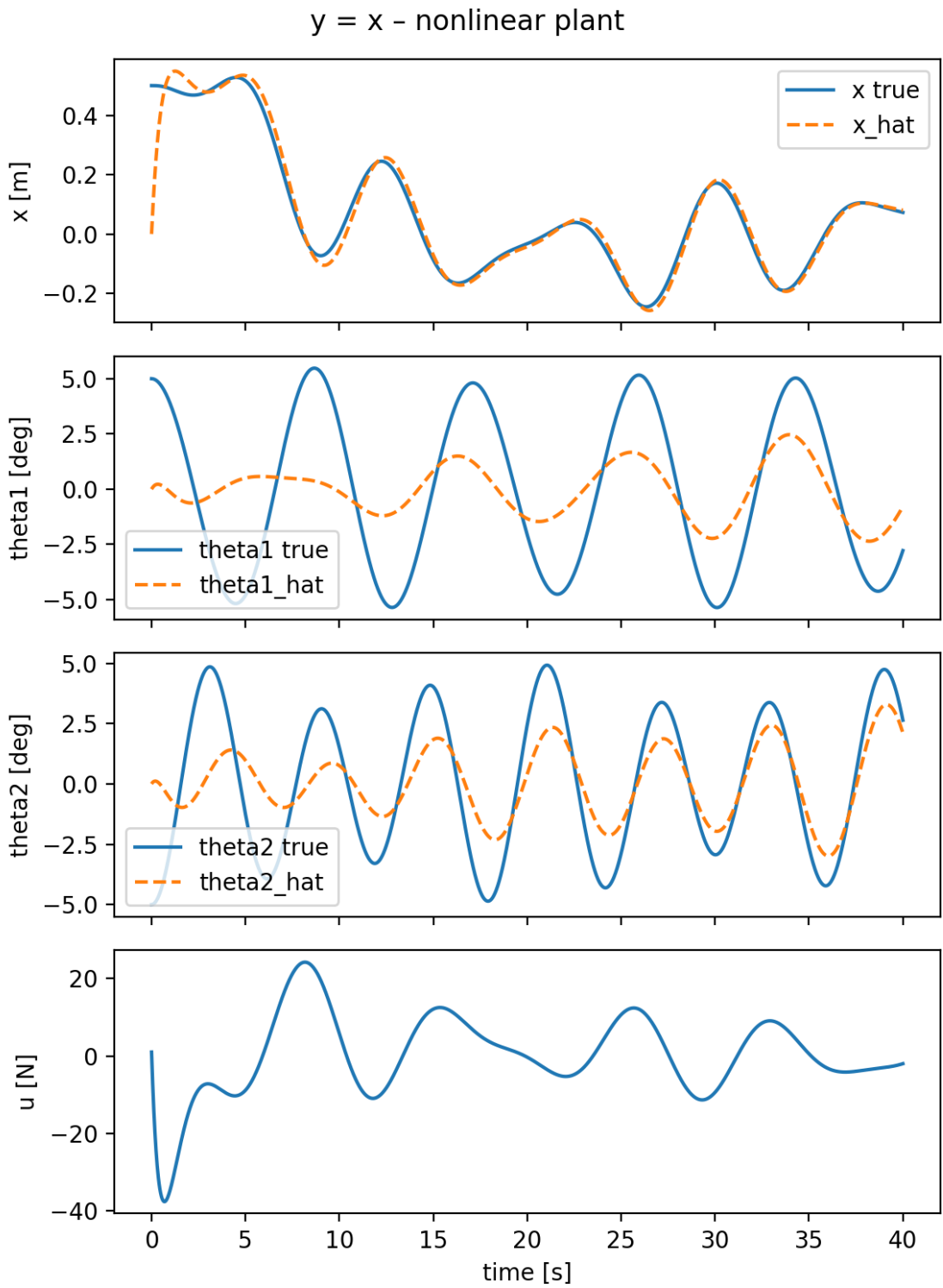


**Figure 8:** Best observer for output  $y = x$  (speed factor  $\alpha = 20$ ), nonlinear plant. The estimation error decays quickly and remains small.

$y = (x, \theta_2)$  - linear plant

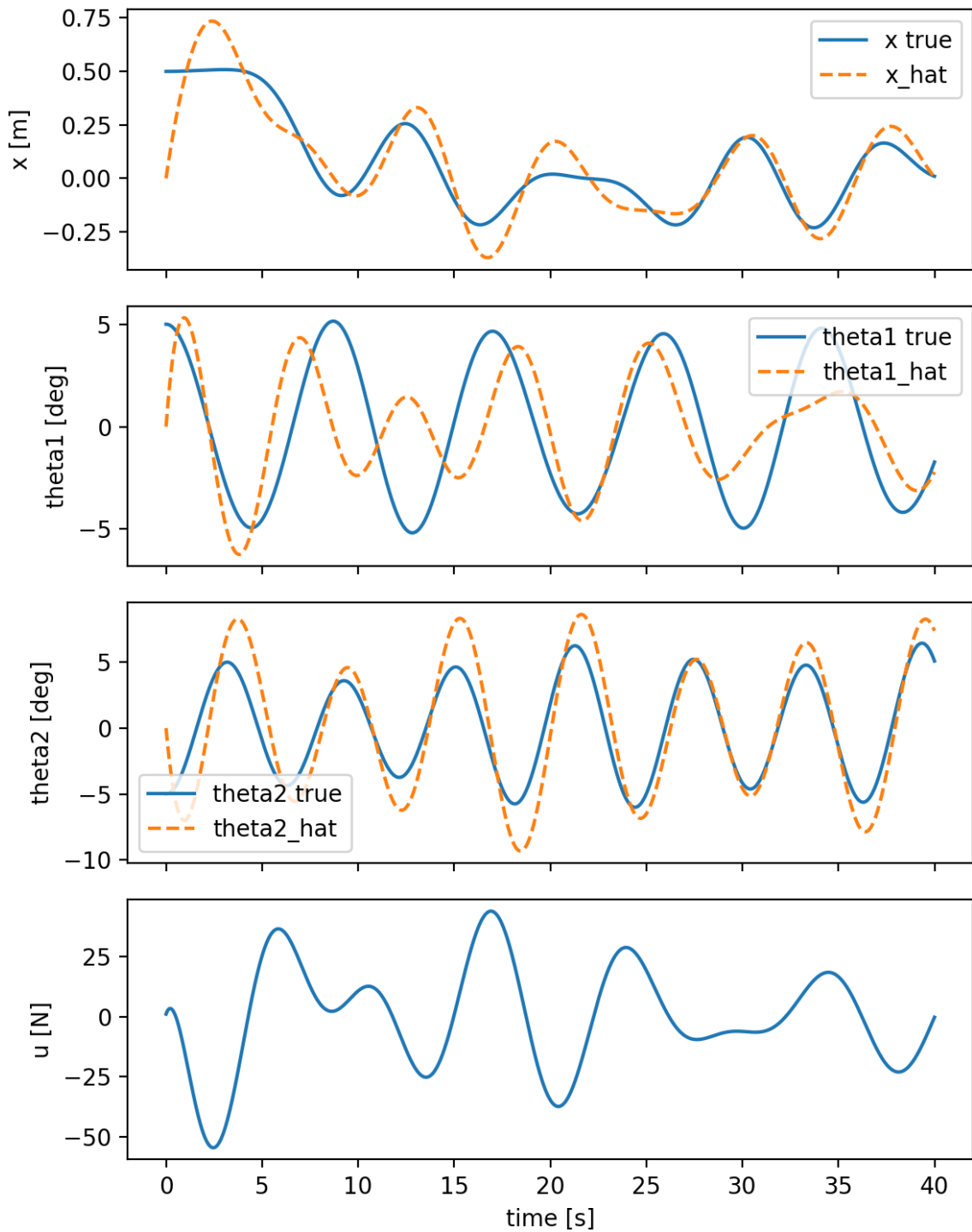


**Figure 9:** Best observer for output  $y = (x, \theta_2)$  (speed factor  $\alpha = 20$ ), linearized plant.

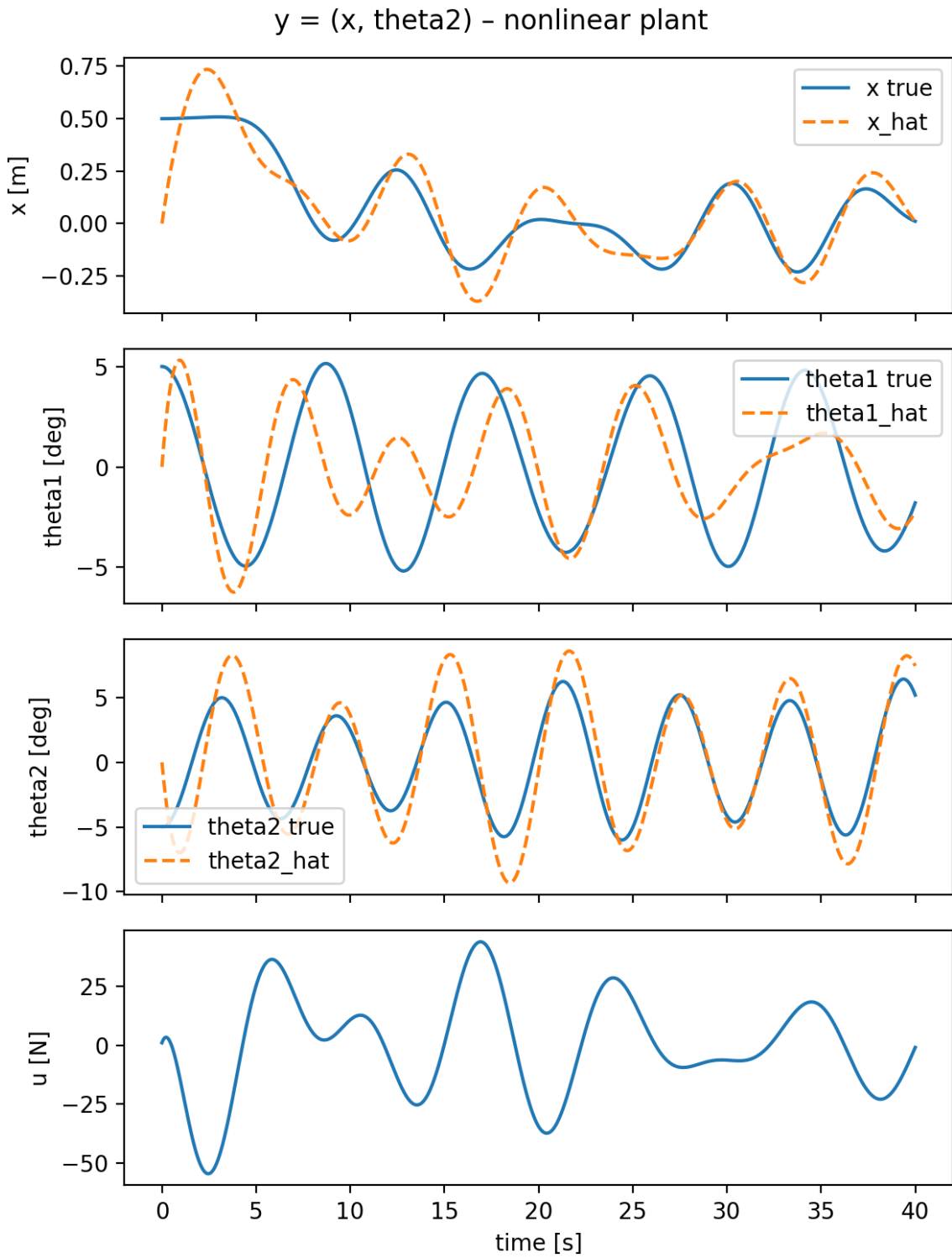


**Figure 10:** Best observer for output  $y = (x, \theta_2)$  (speed factor  $\alpha = 20$ ), nonlinear plant. Measuring  $\theta_2$  improves the reconstruction of both pendulum angles.

$$y = (x, \theta_1, \theta_2) - \text{linear plant}$$

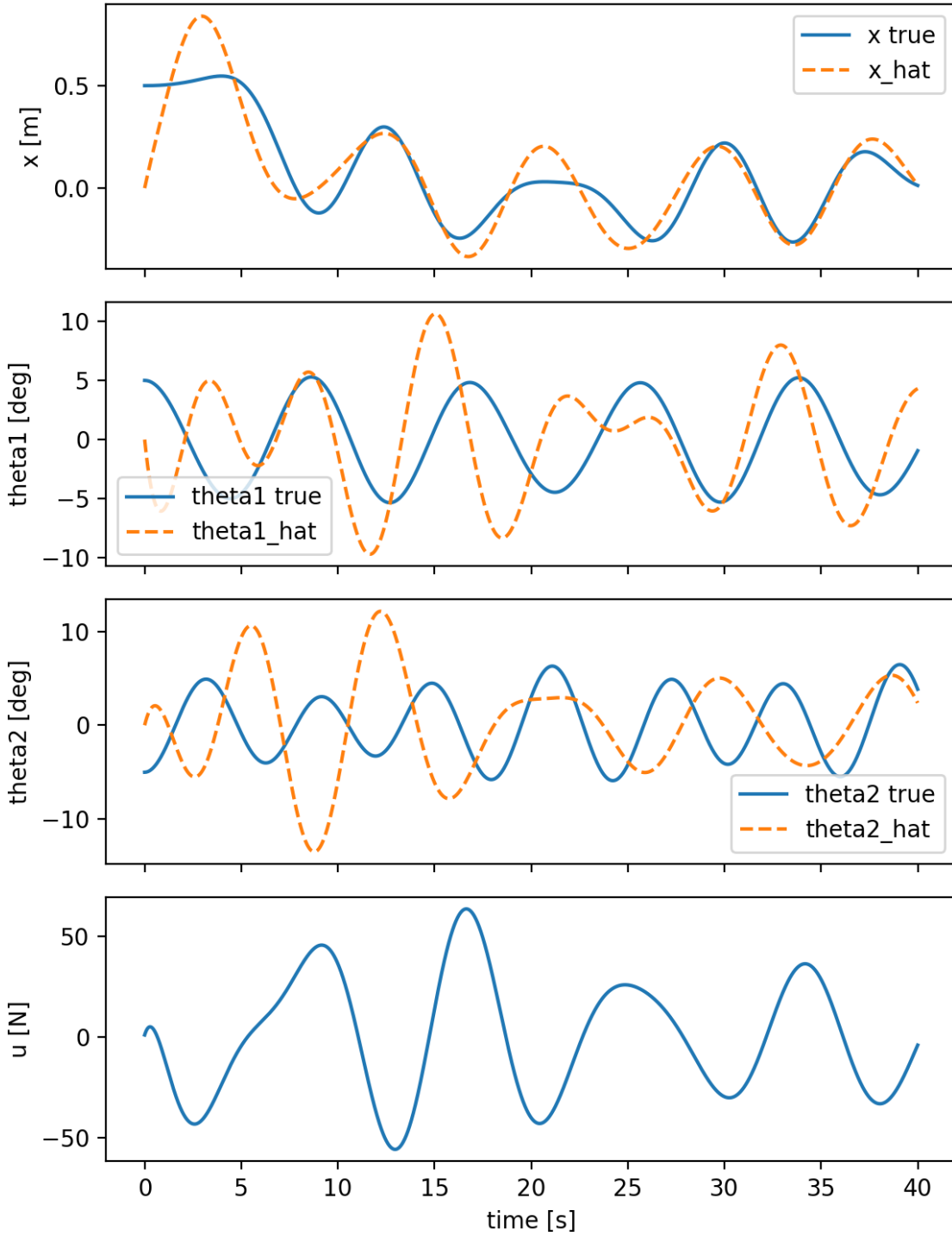


**Figure 11:** Best observer for output  $y = (x, \theta_1, \theta_2)$  (speed factor  $\alpha = 20$ ), linearized plant.

**Figure 12:** Best observer for output  $y = (x, \theta_1, \theta_2)$  (speed factor  $\alpha = 20$ ), nonlinear plant. Using all three measured coordinates yields the smallest estimation ISE, at the expense of a larger control amplitude.

and the output matrix corresponding to  $y = (x, \theta_1, \theta_2)$ :

$$C = \begin{bmatrix} 1 & 0 & 0 & 0 & 0 & 0 \\ 0 & 0 & 1 & 0 & 0 & 0 \\ 0 & 0 & 0 & 0 & 1 & 0 \end{bmatrix}.$$

## LQG structure (separation principle)

The LQG controller combines:

- an LQR state-feedback law  $u(t) = -K\hat{x}(t)$ , and
- a continuous-time Kalman filter (observer)

$$\dot{\hat{x}}(t) = A\hat{x}(t) + Bu(t) + L(y(t) - C\hat{x}(t)).$$

By the separation principle, the closed-loop stability is determined by the union of eigenvalues of  $(A - BK)$  and  $(A - LC)$ .

## LQR design (Design 2)

For the feedback gain  $K$ , we use the tuned LQR weights from **Design 2**:

$$Q = \text{diag}(1, 0.1, 10, 0.5, 10, 0.5), \quad R = 0.01.$$

The LQR gain is computed from the continuous-time algebraic Riccati equation (CARE),

$$A^T P + PA - PBR^{-1}B^T P + Q = 0, \quad K = R^{-1}B^T P.$$

For this design, the closed-loop eigenvalues are

$$\sigma(A - BK) = \{-0.0645 \pm j0.0646, -0.00176 \pm j1.0430, -0.00100 \pm j0.7285\},$$

and the resulting gain (from simulation output) is

$$K = [10.0000 \quad 154.8557 \quad 9.9636 \quad 204.3054 \quad 4.6099 \quad 101.3284].$$

## Continuous-time Kalman filter design (separate measurement noise per channel)

To construct the observer gain  $L$ , we assume process and measurement noise:

$$\begin{aligned} \dot{x}(t) &= Ax(t) + Bu(t) + Gw(t), \\ y(t) &= Cx(t) + v(t), \end{aligned}$$

where  $w(t)$  and  $v(t)$  are zero-mean white noise processes. Following our implementation, we model process noise entering through the same channel as the input:

$$G = B, \quad Q_w = \sigma_w^2,$$

with

$$\sigma_w = 1.0.$$

Measurement noise is configured *separately* for each output component, using

$$\sigma_v = [\sigma_x, \sigma_{\theta_1}, \sigma_{\theta_2}],$$

with the tuned values used in our best simulation:

$$\sigma_x = 0.02 \text{ m}, \quad \sigma_{\theta_1} = 1.0^\circ, \quad \sigma_{\theta_2} = 1.0^\circ.$$

After converting degrees to radians for the filter covariance, the measurement covariance is

$$R_v = \text{diag}(\sigma_x^2, \sigma_{\theta_1}^2, \sigma_{\theta_2}^2) = \begin{bmatrix} 0.0004 & 0 & 0 \\ 0 & 0.00030462 & 0 \\ 0 & 0 & 0.00030462 \end{bmatrix}.$$

The Kalman gain is obtained from the dual CARE,

$$AP_k + P_k A^\top - P_k C^\top R_v^{-1} C P_k + G Q_w G^\top = 0, \quad L = P_k C^\top R_v^{-1}.$$

For the above  $(Q_w, R_v)$ , the computed observer gain (from simulation output) is

$$L = \begin{bmatrix} 2.9382 \times 10^{-1} & -3.1301 \times 10^{-3} & -3.7892 \times 10^{-3} \\ 4.3175 \times 10^{-2} & -1.7992 \times 10^{-4} & -2.4567 \times 10^{-4} \\ -2.3837 \times 10^{-3} & 1.9376 \times 10^{-3} & 5.8829 \times 10^{-5} \\ -5.6815 \times 10^{-4} & 5.6094 \times 10^{-6} & 1.7632 \times 10^{-5} \\ -2.8856 \times 10^{-3} & 5.8829 \times 10^{-5} & 4.5195 \times 10^{-3} \\ -6.7395 \times 10^{-4} & -8.2197 \times 10^{-6} & 1.5682 \times 10^{-5} \end{bmatrix}.$$

## Nonlinear plant application and simulation setup

The same output-feedback law is applied to the **original nonlinear** cart–double-pendulum model:

$$u(t) = -K\hat{x}(t), \quad \dot{\hat{x}}(t) = A\hat{x}(t) + Bu(t) + L(y(t) - C\hat{x}(t)),$$

where  $y(t) = Cx(t) + v(t)$  is generated from the true nonlinear state with additive measurement noise.

The simulation settings are:

- Time horizon:  $T = 40$  s, timestep:  $\Delta t = 0.01$  s (RK4 integration).

- Initial condition:

$$x(0) = [0.5 \ 0 \ 5^\circ \ 0 \ -5^\circ \ 0]^\top.$$

- Measurement noise:  $\sigma_x = 0.02$  m,  $\sigma_{\theta_1} = 1^\circ$ ,  $\sigma_{\theta_2} = 1^\circ$ .

- Process noise:  $\sigma_w = 1.0$ , injected as an additive force through the same channel as  $u$ .

## Simulation results (linear vs. nonlinear)

Figures 13–16 show the simulation results for both plants. With the chosen output  $y = (x, \theta_1, \theta_2)$  and the LQG gains above, the estimated outputs closely match the true outputs, and the unmeasured velocities are also reconstructed accurately. The same controller/observer pair remains stable when applied to the nonlinear dynamics, and the closed-loop trajectories are well-behaved.

## Tracking a constant reference on $x$ (reference reconfiguration)

The LQG regulator designed above is a *regulation* controller: it drives the state to the origin under the nominal model. To track a constant cart-position reference  $x_{\text{ref}}$  (i.e.,  $x(t) \rightarrow x_{\text{ref}}$ ), we reconfigure the control objective from driving  $x(t) \rightarrow 0$  to driving the *tracking error* to zero.

A standard approach is to define the error coordinate

$$e_x(t) = x(t) - x_{\text{ref}},$$

and treat  $(e_x, \dot{e}_x, \theta_1, \dot{\theta}_1, \theta_2, \dot{\theta}_2)$  as the regulated variables. Practically, this is implemented by feeding the reference into the controller in a way that makes the equilibrium correspond to  $x_{\text{ref}}$  rather than 0. For example, one may use a prefilter or reference feedforward term:

$$u(t) = -K\hat{x}(t) + N x_{\text{ref}},$$

where  $N$  is selected so that the steady-state gain from  $x_{\text{ref}}$  to  $x$  is unity for the closed-loop linear model (when such a static mapping is well-defined). This reconfiguration changes the equilibrium point of the closed loop and enables tracking of a constant reference, but it does not by itself guarantee zero steady-state error in the presence of constant input disturbances or modeling mismatch.

LQG ( $y = x, \theta_1, \theta_2$ ) - Linear plant (true vs hat)

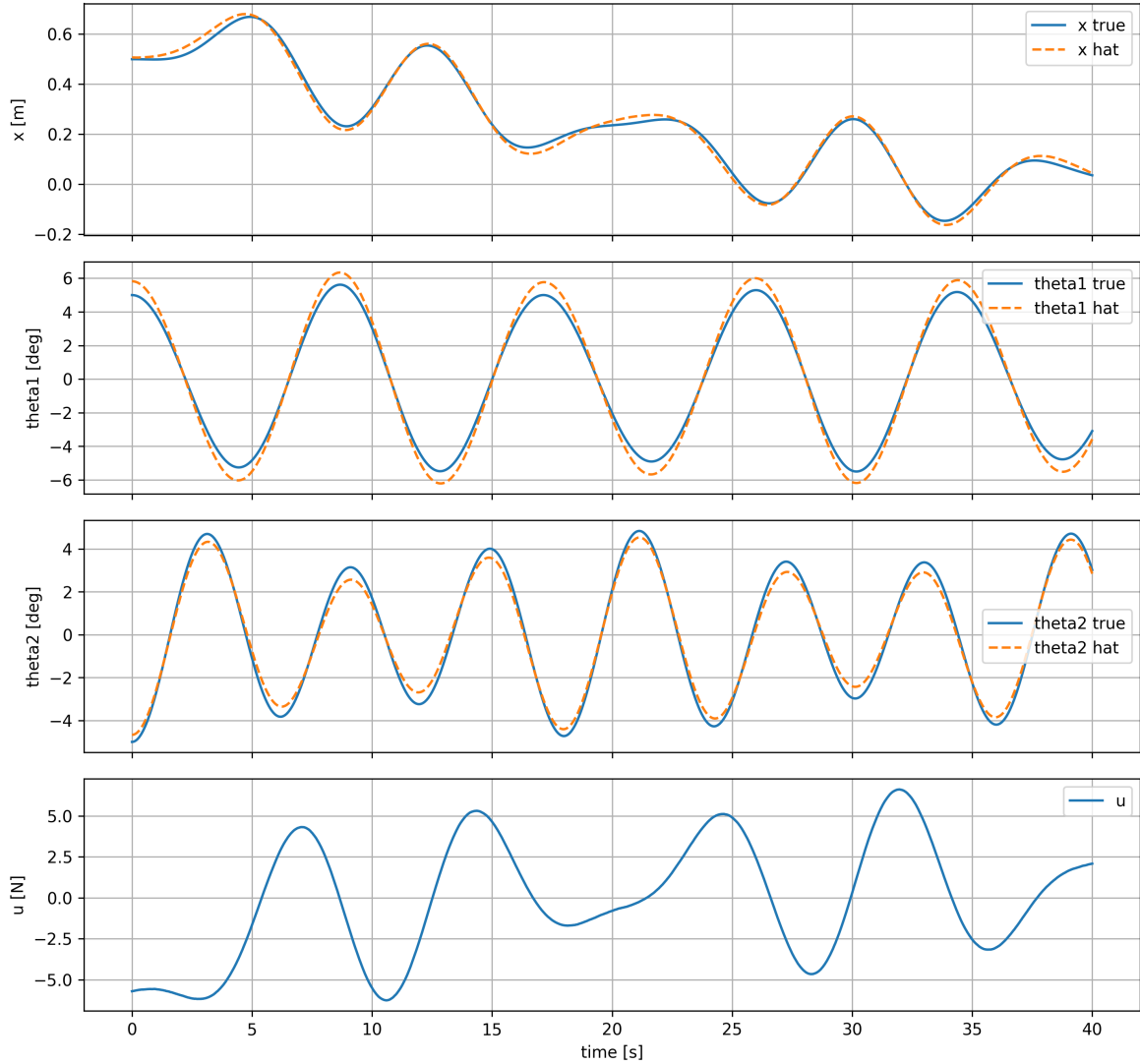


**Figure 13:** LQG output feedback with  $y = (x, \theta_1, \theta_2)$  on the **linearized** plant. Shown: true vs. estimated outputs and the control input  $u(t)$ .

LQG ( $y = x$ ,  $\theta_1$ ,  $\theta_2$ ) - Linear plant (all states true vs hat)

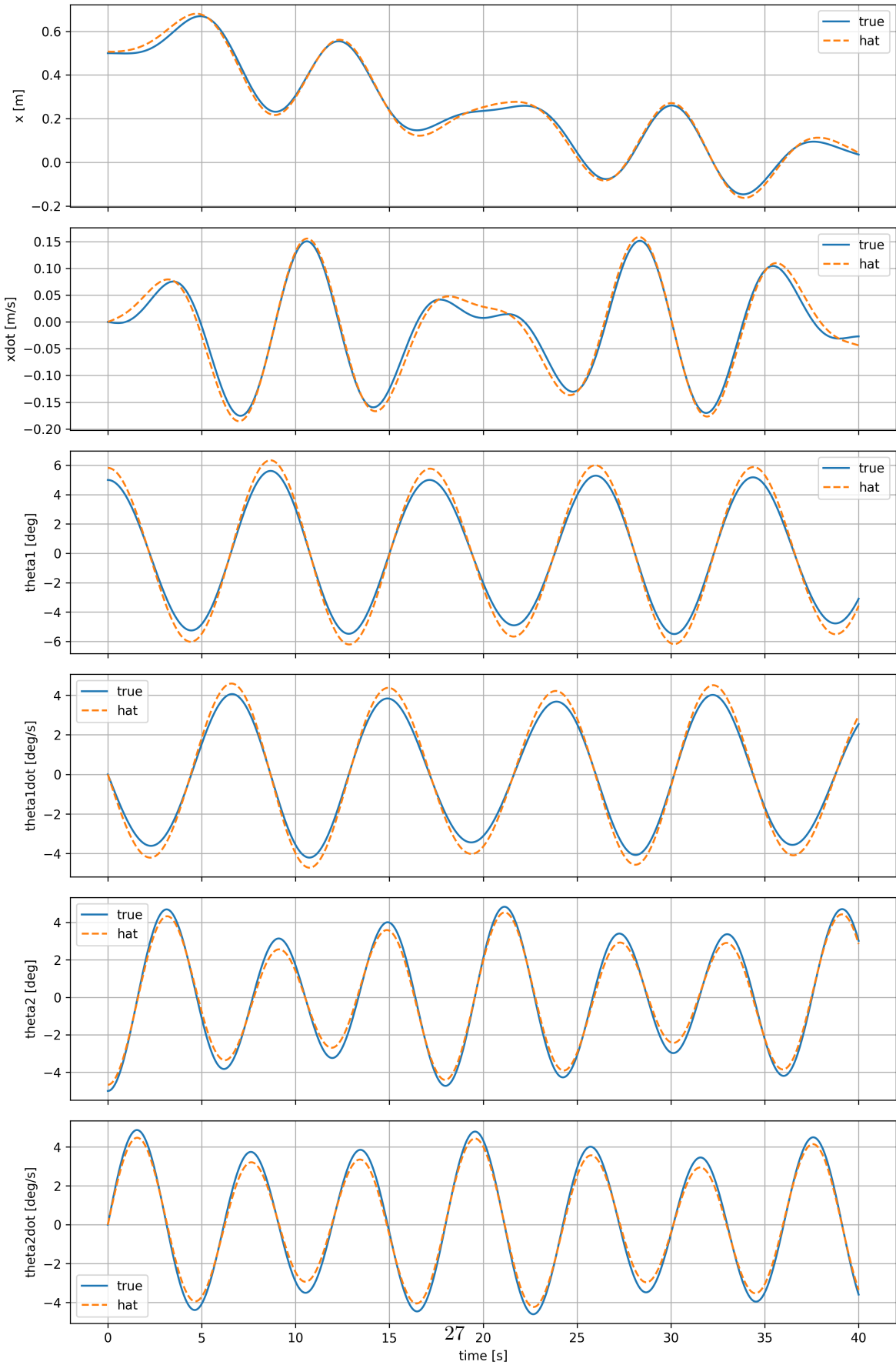


**Figure 14:** LQG output feedback with  $u = (x, \theta_1, \theta_2)$  on the **linearized** plant. Shown: true vs. estimated

LQG ( $y = (x, \theta_1, \theta_2)$ ) - Nonlinear plant (true vs hat)

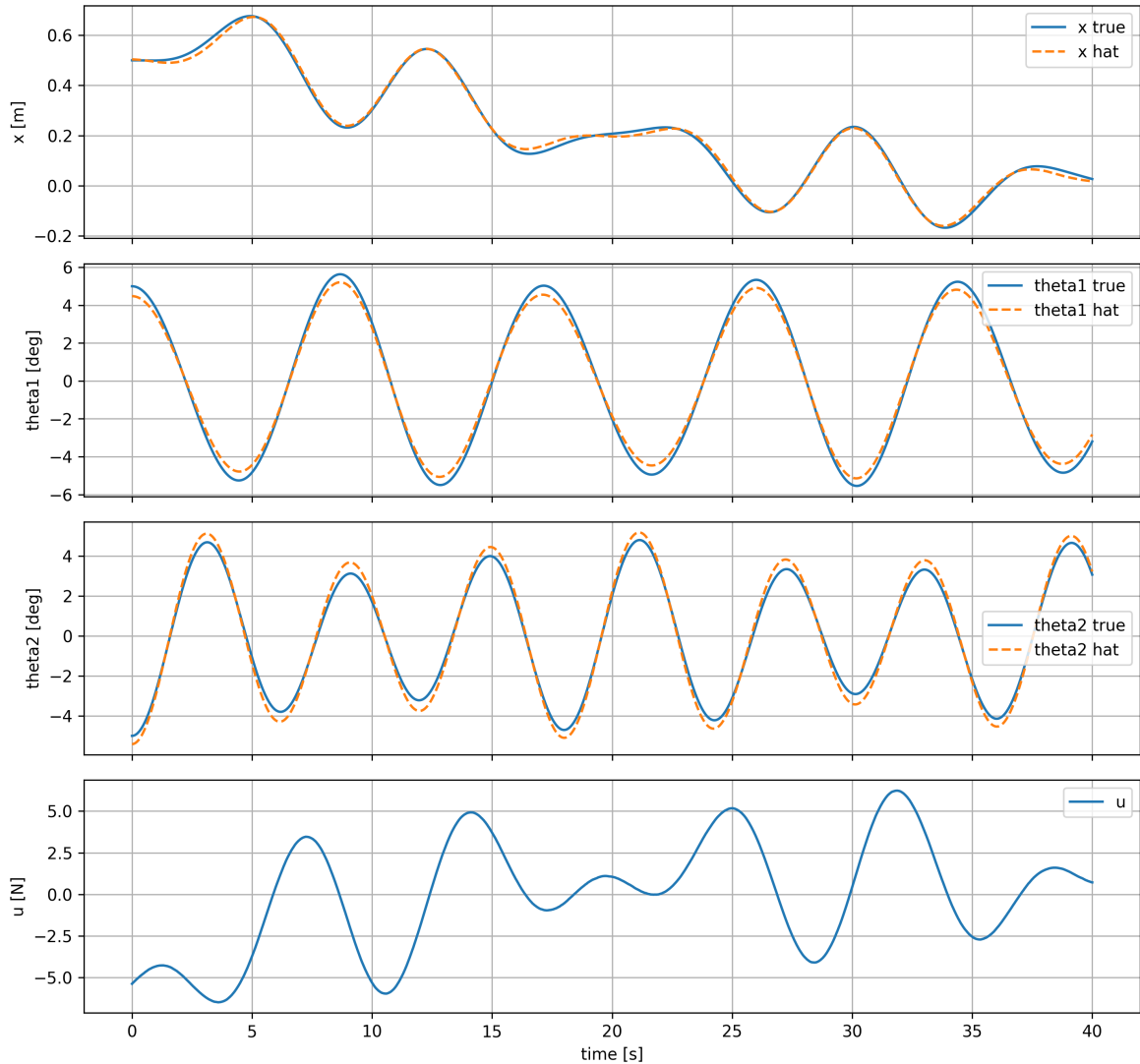


**Figure 15:** LQG output feedback with  $y = (x, \theta_1, \theta_2)$  on the **nonlinear** plant. Shown: true vs. estimated outputs and the control input  $u(t)$ .

LQG ( $y = x, \theta_1, \theta_2$ ) - Nonlinear plant (all states true vs hat)

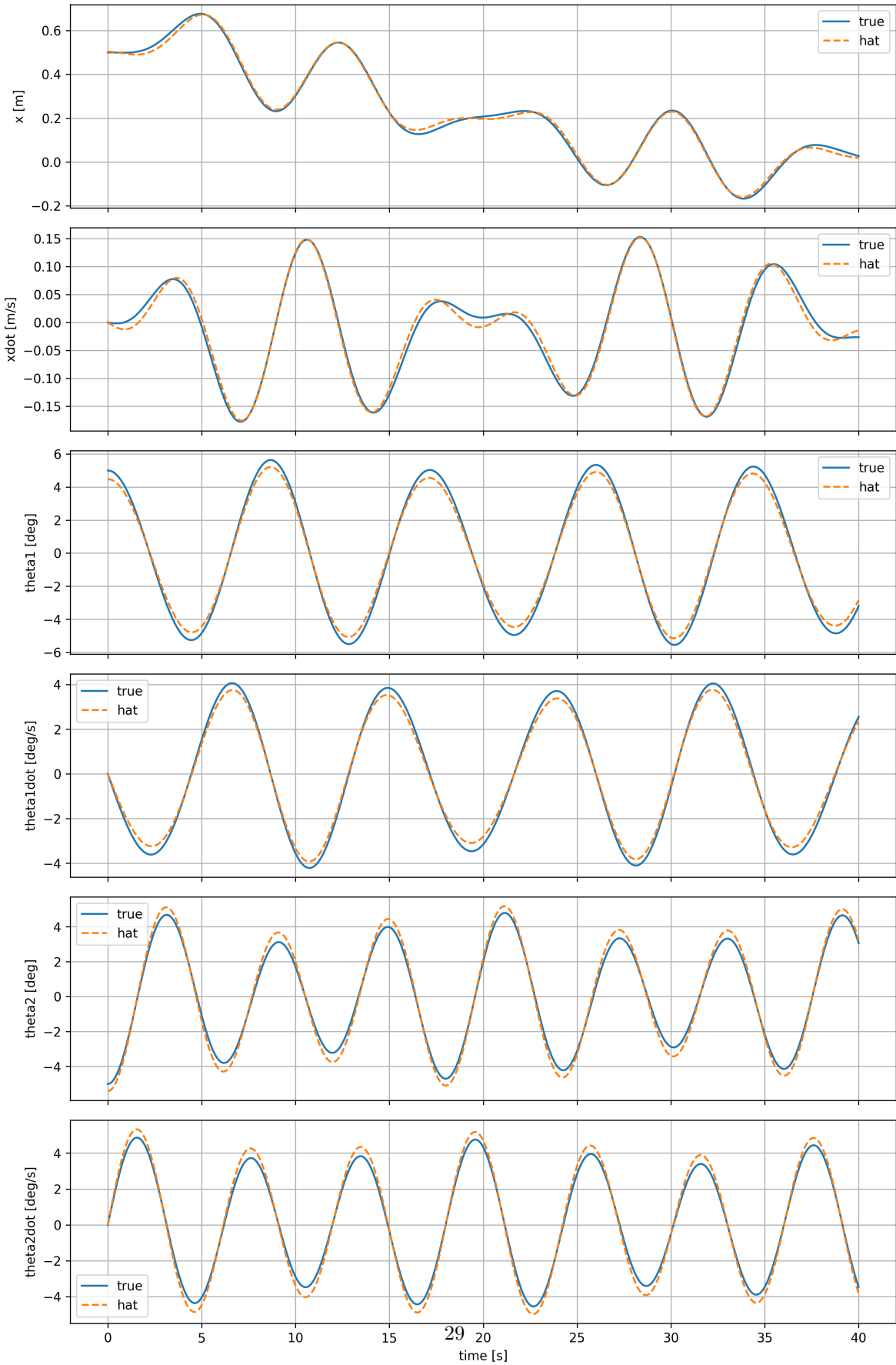


**Figure 16:** LQG output feedback with  $u = (r, \theta_1, \theta_2)$  on the **nonlinear** plant. Shown: true vs. estimated

## Rejection of constant force disturbances (integral augmentation)

A constant unknown force disturbance applied on the cart enters the dynamics as

$$\dot{x}(t) = Ax(t) + B(u(t) + d_0), \quad d_0 = \text{constant}.$$

A standard LQG regulator (without integral action) generally exhibits a nonzero steady-state offset under such a disturbance. To guarantee asymptotic rejection of constant disturbances and enforce zero steady-state tracking error, we augment the controller with an integrator on the cart-position error:

$$z(t) = \int_0^t (x(\tau) - x_{\text{ref}}) d\tau, \quad \dot{z}(t) = x(t) - x_{\text{ref}}.$$

The control law is then modified to include integral feedback,

$$u(t) = -K\hat{x}(t) - K_i z(t),$$

where  $K_i$  is designed (e.g., via LQI by augmenting the linear plant with the integrator state  $z$ ). This augmentation embeds the internal model of a constant signal and allows the closed loop to drive  $x(t) \rightarrow x_{\text{ref}}$  and reject constant force disturbances  $d_0$ .

Because the state has been augmented, the design must be re-validated on the augmented pair  $(A_{\text{aug}}, B_{\text{aug}})$ : in particular, one must check that the augmented system remains stabilizable/controllable (and that the chosen output remains detectable for the estimator), otherwise an asymptotic tracking/disturbance-rejection design may not be achievable.